

1 **A novel cell culture system modeling the SARS-CoV-2 life cycle**

2 Xiaohui Ju¹, Yunkai Zhu², Yuyan Wang², Jingrui Li³, Jiaying Zhang⁴, Mingli Gong¹,
3 Wenlin Ren¹, Sai Li^{4,5}, Jin Zhong⁶, Qiangfeng Cliff Zhang^{4,5}, Rong Zhang², Qiang
4 Ding^{1,5*}

5

6 ¹ School of Medicine, Tsinghua University, Beijing 100084, China

7 ² Key Laboratory of Medical Molecular Virology (MOE/NHC/CAMS), School of Basic
8 Medical Sciences, Shanghai Medical College, Biosafety Level 3 Laboratory, Fudan
9 University, Shanghai 200032, China

10 ³ State Key Laboratory of Plant Physiology and Biochemistry, College of Biological
11 Sciences, China Agricultural University, Beijing 100193, China

12 ⁴ School of Life Sciences, Tsinghua University, Beijing 100084, China

13 ⁵ Beijing Advanced Innovation Center for Structural Biology, Tsinghua University,
14 Beijing 100084, China

15 ⁶ Unit of Viral Hepatitis, CAS Key Laboratory of Molecular Virology and Immunology,
16 Institut Pasteur of Shanghai, Chinese Academy of Sciences, Shanghai, 200031, China

17

18 *Correspondence to Qiang Ding, qding@tsinghua.edu.cn

19

20

21 ABSTRACT

22 Severe acute respiratory syndrome coronavirus 2 (SARS-CoV-2) causes the global
23 pandemic of COVID-19, and no effective antiviral agents and vaccines are available.
24 SARS-CoV-2 is classified as a biosafety level-3 (BLS-3) agent, impeding the basic
25 research into its biology and the development of effective antivirals. Here, we
26 developed a biosafety level-2 (BSL-2) cell culture system for production of
27 transcription and replication-competent SARS-CoV-2 virus-like-particles (trVLP). This
28 trVLP expresses a reporter gene (GFP) replacing viral nucleocapsid gene (N), which is
29 required for viral genome packaging and virion assembly (SARS-CoV-2-GFP/ Δ N
30 trVLP). The complete viral life cycle can be achieved and exclusively confined in the
31 cells ectopically expressing SARS-CoV or SARS-CoV-2 N proteins, but not MERS-
32 CoV N. Genetic recombination of N supplied *in trans* into viral genome was not
33 detected, as evidenced by sequence analysis after one-month serial passages in the N-
34 expressing cells. Moreover, intein-mediated protein trans-splicing approach was
35 utilized to split the viral N gene into two independent vectors, and the ligated viral N
36 protein could function *in trans* to recapitulate entire viral life cycle, further securing the
37 biosafety of this cell culture model. Based on this BSL-2 SARS-CoV-2 cell culture
38 model, we developed a 96-well format high throughput screening for antivirals
39 discovery. We identified salinomycin, tubeimoside I, monensin sodium, lycorine
40 chloride and nigericin sodium as potent antivirals against SARS-CoV-2 infection.
41 Collectively, we developed a convenient and efficient SARS-CoV-2 reverse genetics
42 tool to dissect the virus life cycle under a BSL-2 condition. This powerful tool should
43 accelerate our understanding of SARS-CoV-2 biology and its antiviral development.

44

45 **Key words:** SARS-CoV-2, COVID-19, Reverse genetics, intein, drug screening.

46

47

48 INTRODUCTION

49 The coronavirus disease 2019 (COVID-19) caused by severe acute respiratory
50 syndrome coronavirus 2 (SARS-CoV-2) is an ongoing pandemic¹. As of 1 December
51 2020, more than 63.7 million cases of COVID-19 have been reported, resulting in more
52 than 1.5 million deaths. Severe patients died of breathing difficulty to acute respiratory
53 distress. Up to now, there is still no vaccine and antiviral agents available².

54 SARS-CoV-2 belongs to the genus *Coronavirus*, the family *Coronaviridae*, and
55 the order *Nidovirales*. Its genome is a single-stranded, positive-sense RNA with similar
56 specific gene characteristics of known coronaviruses³. The viral genome encodes non-
57 structural proteins, structural proteins and accessory proteins. The non-structural
58 proteins carry all of the enzymatic activities important for viral replication. For example,
59 the genome encodes an RNA-dependent RNA-polymerase complex (nsp7, nsp8 and
60 nsp12), RNA capping machinery (nsp10, nsp13, nsp14 and 16) and additional enzymes
61 such as proteases (the nsp3 PLpro and the nsp5 3CLpro) which cleave viral
62 polyproteins^{4,5}. Structural proteins include surface (S), envelope (E), membrane (M),
63 and nucleocapsid (N) proteins⁶. The S, E and M proteins are embedded within the lipid
64 envelope. The primary function of N protein is to package the ~30 kb single stranded,
65 5'-capped positive-strand viral genome RNA into a ribonucleoprotein (RNP) complex.
66 Ribonucleocapsid packaging is a fundamental part of viral self-assembly, and the RNP
67 complex constitutes the essential template for replication by the RNA-dependent RNA
68 polymerase complex⁷. In addition, the N protein has been shown to modulate the host
69 antiviral response and may play regulatory roles in the viral life cycle³. The accessory
70 proteins, encoded by ORF3a, ORF6, ORF7a, ORF7b, and ORF8 genes, are not directly
71 involved in viral replication but interfere with the host innate immune response or are
72 of unknown function^{3,8,9}.

73 The development of reverse genetics systems of coronavirus has profoundly
74 advanced the study of this large-sized RNA virus. The cDNA of the coronavirus RNA
75 genome is constructed using bacterial artificial chromosomes (BACs), in vitro ligation
76 of CoV cDNA fragments, or vaccinia viral vector¹⁰. Recently, a SARS-CoV-2 full-

77 length cDNA clone has been established using the *in vitro* ligation of cDNA
78 fragments^{11,12}. This system has been shown to be efficient for the recovery of infectious
79 virus, and a reporter gene can be inserted into the viral genome to monitor virus
80 replication, providing a good tool for high-throughput antiviral screening. However,
81 experimentations involving live virus are restricted to BSL-3 laboratories, which
82 hinders the study of SARS-CoV-2 and development of countermeasures. Therefore, it
83 is urgent to develop an efficient non-BSL-3 experimental system for SARS-CoV-2.
84 Herein, we developed an N-based genetic complementation system to produce
85 biologically contained, and transcription, replication-competent SARS-CoV-2 virus-
86 like particles lacking N gene (SARS-CoV-2 Δ N trVLP). The lack of the viral N protein
87 could be genetically complemented *in trans* by ectopic expression in packaging cells to
88 produce the SARS-CoV-2 Δ N trVLP. SARS-CoV-2 Δ N trVLP could be propagated and
89 passaged in the packaging cells while only results in single-round infection in wild-type
90 cells. We applied this cell culture model for SARS-CoV-2 biology, antiviral evaluation
91 and novel antivirals discovery.

92

93 **RESULTS**

94 **Design and assembly of SARS-CoV-2-GFP/ Δ N genome**

95 Nucleocapsid translated from a subgenomic RNA of SARS-CoV-2 has multiple
96 functions and its primary function is participation in genomic RNA package and virus
97 particle release. To test whether the function of N could be complemented *in trans*, we
98 constructed SARS-CoV-2-GFP/ Δ N genome, in which we replaced the regions encoding
99 viral N (from nucleotides position 28274 to 29533) based on MN908947 genome with
100 GFP reporter gene, and Caco-2 cells, an immortalized cell line of human colorectal
101 adenocarcinoma cells, as packaging cell lines which stably express viral N protein by
102 lentiviral transduction (**Fig. 1**).

103 To assemble the molecular clone of SARS-CoV-2-GFP/ Δ N genome, we utilized
104 an *in vitro* ligation approach, which has been used for constructing the infectious clone
105 of SARS-CoV-2^{11,12}. We divided the full-length cDNA of SARS-CoV-2-GFP/ Δ N
106 genome into a set of five fragments (A, B, C, D and E) and each fragment can be
107 obtained by PCR using the chemically synthesized viral genome (MN908947 strain) as
108 the template. Each DNA fragment was flanked by a type IIS restriction endonuclease
109 site (BsaI or BsmBI) that ensures unidirectional assembly of intermediates into a full-
110 length cDNA. In addition, we engineered a T7 promoter upstream of fragment A and a
111 poly(A) tails at the downstream of fragment E, allowing for *in vitro* transcription of
112 capped, polyadenylated transcript of viral genome (**Fig. 1A**).

113 The five PCR-amplified DNA fragments were digested with BsaI or BsmBI to
114 generate specific sticky ends (**Fig. 1B**). The digested fragments were further purified
115 and were ligated by T4 DNA ligase at 4°C to generate the full-length cDNA of SARS-
116 CoV-2-GFP/ Δ N genome. The resulting 29.4-Kbp *in vitro* ligation products were
117 confirmed by agarose gel electrophoresis (**Fig. 1C**). Next, this *in vitro* ligation products
118 were used as the template for *in vitro* transcription with the T7 RNA polymerase to
119 generate the RNA transcript of SARS-CoV-2-GFP/ Δ N genome (**Fig. 1D**).

120 **Recovery and propagation of SARS-CoV-2-GFP/ Δ N trVLP**

121 Caco-2 cells are highly permissive for SARS-CoV-2 infection. As the recombinant

122 SARS-CoV-2-GFP/ Δ N virus like particles, lacking N gene, could potentially propagate
123 in the cells supplied with viral N protein *in trans*, we established the Caco-2 cells stably
124 expressing viral N gene by lentiviral transduction (designated as Caco-2-N cells). The
125 expression of N was confirmed by flow cytometry and immunoblotting assay (**Fig. S1A,**
126 **B and Fig. 1E**).

127 Next, we sought to recover SARS-CoV-2-GFP/ Δ N trVLP, the *in vitro* transcribed
128 RNA transcript of viral genome was electroporated into Caco-2-N cells. Within 48h,
129 GFP fluorescence can be readily observed, suggesting that viral genome replication and
130 transcription occurs in the cell. After 96h, cytopathic effects (CPEs) were observed in
131 the electroporated Caco-2-N cells, suggesting that the recombinant SARS-CoV-2-
132 GFP/ Δ N trVLP was produced and propagated (**Fig. S2**). We collected the cell culture
133 supernatants (denoted as passage 0 (P0) virus), and inoculated them to Caco-2 or Caco-
134 2-N cells (**Fig. 2A**). GFP signal can be readily observed within 48 h, and further
135 expanded within 72 h in Caco-2-N cells, whereas no signal was detected in Caco-2 cells
136 (**Fig. 2B**). Cells were collected for immunoblotting and RT-qPCR analysis at 72 h post-
137 infection to detect viral spike antigen and RNA abundance. Consistent with the GFP
138 expression, we could detect viral spike expression and high abundance of viral RNA in
139 the Caco-2-N cells but not in Caco-2 cells (**Fig. 2C and D**). RT-PCR analysis using a
140 primer set outside the N-encoding region confirmed that the N gene was indeed
141 replaced by GFP in the recombinant trVLP viral genome (**Fig. 2E**).

142 To characterize the SARS-CoV-2-GFP/ Δ N trVLP infection, two spike-specific
143 mAbs (1F11 and 2F6)¹³ were tested for their ability to neutralize infection of Caco-2-
144 N cells. A neutralizing mAb specific for HIV gp120 (VRC-01) was also included as the
145 control¹⁴. The mAbs were incubated with SARS-CoV-2-GFP/ Δ N trVLP for 1 h at 37°C,
146 and the trVLP–mAb mixtures were tested for infection of Caco-2-N cells, respectively.
147 Viral infection was determined by flow cytometry at 48 h post-infection, and the results
148 showed that 1F11 and 2F6 inhibited trVLP infection in a dose-dependent manner; in
149 contrast, VRC01 had no effect on the trVLP infection (**Fig. 2F**).

150 Soluble recombinant forms of the human ACE2 are able to bind SARS-CoV-2

151 spike protein and inhibit its interaction with cellular ACE2^{15,16}. We therefore tested the
152 ability of mouse IgG Fc fusion proteins of soluble human ACE2 (D30E) (hACE2
153 (D30E)-Fc)¹⁶ to inhibit SARS-CoV-2-GFP/ Δ N trVLP infection. F10scFv, an antibody
154 specifically targeting HA of the Influenza A virus, was used as a negative control. The
155 hACE2 (D30E)-Fc trVLP showed a dose-dependent neutralization of infectivity,
156 inhibiting SARS-CoV-2-GFP/ Δ N infection of Caco-2-N cells by 70% at 0.5 μ g/ml (**Fig**
157 **2G**). Together, these data demonstrated that the infection of SARS-CoV-2-GFP/ Δ N
158 trVLP recapitulates that of wild-type virus as its virus entry is also mediated by the
159 interaction between viral spike and host ACE2.

160 **Characterization of the genetic stability of SARS-CoV-2-GFP/ Δ N trVLP**

161 Next, we sought to characterize the genetic stability of SARS-CoV-2-GFP/ Δ N
162 trVLP. For this purpose, we analyzed the rescued SARS-CoV-2-GFP/ Δ N trVLP in
163 Caco-2-N cells after 10 passage. The cell culture supernatants collected from SARS-
164 CoV-2-GFP/ Δ N RNA electroporated Caco-2-N cells were defined as P0, and the cell
165 cultures collected from each subsequent passage on the Caco-2-N cells were defined as
166 P1 to P10, respectively. The total RNAs extracted from each cell passage were used to
167 perform RT-PCRs with the pair of primers to amplify the fragment between ORF8 and
168 3'UTR that covers the region of the inserted GFP reporter gene. (**Fig.3A**). RT-PCR
169 products of 1.5-Kbp and 1-Kbp were expected for WT genome and SARS-CoV-2-
170 GFP/ Δ N genome, respectively. SARS-CoV-2-GFP/ Δ N trVLP was considerably stable
171 for at least 3 serial passages since the 1-Kb RT-PCR products were detected at P3 trVLP
172 (**Fig. 3B**). The loss of GFP reporter gene was detected in the P4 trVLP as indicated by
173 amplicon of < 1 Kb size (**Fig. 3B, Fig S3A**). No PCR product of greater than 1 Kb was
174 detected in the all samples, suggesting that no heterologous RNA inserted into the
175 SARS-CoV-2-GFP/ Δ N genome, at least in the GFP report region.

176 To characterize the trVLP sequence variations in an unbiased manner, we
177 performed deep sequencing analysis on the P1 and P10 trVLP genome. The deep
178 sequencing analysis provides deep coverage, on the order of 30 million reads per
179 sequencing sample (**Fig. S3B**). Sequences of P1 or P10 were mapped to the SARS-

180 CoV-2 and SARS-CoV-2-GFP/ Δ N trVLP genomes, respectively (**Fig. 3C and D**) and
181 relative abundances of these sequences between P1 and P10, were also compared (**Fig**
182 **3E, Fig S3C**). The deep sequencing analysis could not detect N sequences in the both
183 P0 and P10 genome (**Fig. 3C**), and GFP sequences were readily detected in the P1
184 genome with high abundance, however, it was rarely detected in the P10 genome (**Fig.**
185 **3D**), due to GFP sequences deletion (**Fig. 3B, Fig S3A**). Additionally, we found that
186 the subgenomic RNAs of ORF6, ORF7 and ORF8 were dramatically decreased in the
187 P10-trVLP infected cells compared with that of P1 VLP (**Fig. 3E**), indicating that ORF6,
188 ORF7 and ORF8 may not be required for virus infection at least *in vitro*, consistent with
189 other reports that deletions of these regions were observed in clinical samples by deep
190 sequencing analysis¹⁷⁻²⁰.

191 **Reconstitution of functional N protein by split intein-mediated protein ligation**

192 Inteins are intervening protein sequences within a host protein that mediate their
193 self-excision from the precursor protein and ligates the flanking N- and C-terminal
194 fragments (exteins)²¹. Split inteins are a subset of inteins that are expressed as two
195 separate polypeptides at the ends of two host proteins and catalyze their trans-splicing,
196 resulting in the generation of a single larger polypeptide (**Fig. 4A**). To further minimize
197 the chance of recombination of N into the SARS-CoV-2-GFP/ Δ N genome, we aimed
198 to split the N gene into two separate elements using a naturally split intein embedded
199 within the catalytic subunit of DNA polymerase III (DnaE) in many species of
200 cyanobacteria (Npu intein)²². Npu intein activity is context-dependent, and Cys as first
201 residue in the C-extein is required for efficient trans-splicing. However, there is no Cys
202 residue in SARS-CoV-2 N protein. In order to split the N, we had to find the appropriate
203 splice sites that would have two well-folded, yet stable protein fragments, and also
204 substitute first residue in the C-extein with Cys without disruption of N protein function.
205 To locate the splice sites according to these requirements we chose three splice sites in
206 the N protein, to have the N-intein A152C, S176C and G212C (**Fig. 4A**). As for each
207 of N-intein above, we constructed two lentivirus vectors encoding either the N- or the
208 C-terminal half of the N protein fused to the N- and C-terminal halves of the Npu intein,

209 having N^N-Int^N and Int^C-N^C, respectively (**Fig. 4A**). Each lentivirus vector included
210 appropriate regulatory elements (promoter and a polyadenylation signal) and a Flag tag
211 to allow detection of the full-length reconstituted N protein (**Fig. 4A**). We then
212 transduced N^N-Int^N and Int^C-N^C either individually or together in Caco-2 cells, and the
213 full-length N protein reconstitution was assessed by Western blotting assay. We could
214 not detect splicing above negligible levels of N protein by N-intein (A152C) (**lane 2,**
215 **Fig. 4B**), while N-intein (S176C) and N-intein (G212C) could reconstitute into full-
216 length N protein with S176C or G212C point mutation, respectively (**lane 5 and 8, Fig.**
217 **4B**). Next, recombinant SARS-CoV-2 GFP/ Δ N trVLP (P1) was inoculated to Caco-2
218 cells transduced with N-intein as indicated, and GFP fluorescence was detected after
219 two days only in the cells transduced either with a single lentivirus that encodes full-
220 length N or with the combination of N-intein (G212C), but not in the cells with the
221 single N- and C-terminal N-intein (G212C). As expected, GFP fluorescence was also
222 not detected in cells transduced with N-intein (A152C), of which the splicing did not
223 occur; interestingly, N-intein (S176C) could ligate a full-length N (S176C), but fails to
224 support virus infection, suggesting that the S176C mutation probably impairs N protein
225 function (**Fig. 4C and D**). Consistent with the GFP expression, the subgenomic RNA
226 of E can be readily detected in cells transduced either with a single lentivirus that
227 encodes full-length N or with the combination of N-intein (G212C), but not others (**Fig.**
228 **4E**). Together, we showed that the N-intein (G212C) was capable of efficiently trans-
229 splicing to generate a functional N (G212C) protein to support SARS-CoV-2 GFP/ Δ N
230 trVLP infection. As the N-intein was split into separate constructs, it would further
231 reduce the potential biosafety concerns of this SARS-CoV-2 GFP/ Δ N trVLP cell culture
232 model.

233 **Residue-specific phosphorylation of N protein is critical for viral infectivity**

234 Coronavirus N protein is an extensively phosphorylated, highly basic, vital
235 structural protein the primary function of which is to form a helical ribonucleoprotein
236 complex with viral RNA (RNP) as core structure of the virion. A variety of other
237 functions have been ascribed, such as viral genome transcription and replication, or

238 evasion of antiviral immunity. SARS-CoV-2 N protein is highly homologous to the N
239 protein of SARS-CoV, with 91% identity, while exhibited 48% identity with that of
240 MERS-CoV (**Fig. 5A**). Several proteomics profiling analyses have been performed and
241 reveals that N protein of SARS-CoV-2 is extensively phosphorylated at multiple sites
242 (**Fig. 5A and Fig. S4**). However, the roles of N protein phosphorylation remain unclear.
243 Our N-based genetic trans-complemented cell culture model offers an opportunity to
244 specifically study N protein function in viral life cycle. Firstly, we determined whether
245 SARS-CoV-2 GFP/ Δ N trVLP infection can be complemented by N proteins from
246 different coronaviruses. We used SARS-CoV-2 GFP/ Δ N trVLP to infect the Caco-2 cells
247 transduced with N from SARS-CoV-2, SARS-CoV or MERS-CoV. Two days later, the
248 cell culture supernatants from each cells were collected to infect naive Caco-2 cells
249 transduced with SARS-CoV-2 (Caco-2-N cells as previously used) to test whether
250 SARS-CoV-2 GFP/ Δ N trVLP were assembled in the Caco-2 cells transduced with
251 distinct N proteins. Two days later, the Caco-2-N cells were collected and GFP or viral
252 RNA was quantified by flow cytometry or RT-qPCR, respectively (**Fig. 5B and C**).
253 SARS-CoV N protein with 91% identity with that of SARS-CoV-2, but not MERS-
254 CoV N protein with 48% identity with that of SARS-CoV-2, could rescue SARS-CoV-
255 2 GFP/ Δ N trVLP, (**Fig. 5D and E**), suggesting that coronavirus N protein has virus-
256 specific mechanism to recognize viral genome to achieve its function, meanwhile, N
257 proteins from SARS-CoV and SARS-CoV-2, with high genetic similarity, have
258 redundant function to some degree.

259 As SARS-CoV-2 N is heavily phosphorylated at multiple sites especially within
260 the central Ser-Arg (SR)-rich motif, we are interested in the roles of phosphorylation in
261 N function. For this purpose, we mutated S176, S413, S176/413, S105, S183, S188,
262 S206, S188/206 as the conservation of these residues with that of SARS-CoV into
263 alanine to specifically dissect their function. Notably, GSK-3 is the kinase responsible
264 for the phosphorylation of this SR-rich motif in SARS-CoV N protein, which are
265 primed by the phosphorylation of Ser-189 and Ser-207 (Ser-188 and Ser-206 in SARS-
266 CoV-2 N protein accordingly)^{23,24}. We generated the Caco-2 cells lentivirally

267 transduced with the N variants as indicated. As shown in Western blotting assay, the
268 mutations did not alter the protein expression and stability in the Caco-2 cell (**Fig. 5F**),
269 We noted that N with the S188A/S206A double mutations migrated slightly faster than
270 WT and other mutants, probably because blockade of the initial priming
271 phosphorylation would prohibit subsequent phosphorylation events by GSK-3, which
272 was observed in SARS-CoV²³. Next, we inoculated the Caco-2 cells expressing
273 different N variants with SARS-CoV-2 GFP/ Δ N trVLP, and cell culture supernatant was
274 collected 48 h later to infect the naïve Caco-2-N cells, and cells were collected to
275 observe or determine GFP expressing by microscopy or flow cytometry 2 days later.
276 Interestingly, most of the phosphorylation null mutants were able to assemble virus-like
277 particles with comparable or slightly reduced efficiencies than WT. However,
278 S188A/S206A double mutations completely abolish N function (**Fig. 5G-H**),
279 highlighting the critical role of S188 and S206 for N function.

280 To further investigate whether GSK-3 contributing N protein phosphorylation to
281 regulate virus life cycle, we treated Caco-2-N cells with LiCl or SB216763, which are
282 specific inhibitors of GSK-3 and inoculated cells with SARS-CoV-2 trVLP
283 spontaneously. Two days later, cell culture medium was collected and infect Caco-2-N
284 cells for additional 2 days, and then cells were harvested for flow cytometry analysis of
285 GFP expression. As expected, the LiCl or SB216763 could inhibit GFP expression in a
286 dose-dependent manner, indicating that inhibition of GSK-3 could block N
287 phosphorylation, thus impairing SARS-CoV-2 trVLP production. Given the vital role
288 of the N protein in multiple stages of the viral life cycle, inhibition of N functions by
289 modulating host cell kinases may be viable strategies for combating SARS-CoV-2
290 infections.

291 **Evaluation of the antivirals using SARS-CoV-2-GFP/ Δ N VLP cell culture model**

292 To test the utility of this system in anti-viral drug screening, we evaluated the
293 efficacy of IFN- β , remdesivir, GC376, lopinavir, and ritonavir in inhibiting SARS-
294 CoV-2 GFP/ Δ N trVLP infection. Caco-2-N-intein (G212C) cells were treated with IFN-
295 β with 0.2–20 pg/ml for eight hours prior to infection. Then cells were infected with

296 SARS-CoV-2 GFP/ Δ N trVLP at a multiplicity of infection (MOI) of 0.05. After 48 h,
297 the cells were collected and GFP fluorescence, the proxy of virus infection, was
298 quantified by flow cytometry analysis. Remarkably, even at 0.2 pg/ml IFN- β we
299 observed 60% reduction of the GFP fluorescence (**Fig. 6A**). This is consistent with
300 recent reports that SARS-CoV-2 is sensitive to type I interferon treatment^{11,25-27}.
301 Remdesivir and GC376, which targets virus RNA dependent RNA polymerase (RdRp)
302 and 3CLpro respectively, have been reported to be potent antivirals against SARS-CoV-
303 2²⁸⁻³². Lopinavir and ritonavir-HIV protease inhibitor, is a combination antiviral
304 medicine used to treat HIV³³, which could inhibit SARS-CoV and MERS-CoV
305 infection *in vitro*, and they may target SARS-CoV-2 Nsp5 (3CLpro) to inhibit virus
306 infection. To test potential dose-dependent antiviral activity of those drugs in our
307 system, we incubated Caco-2-N-intein (G212C) cells with various concentrations of
308 those drugs and simultaneously infected the cells with SARS-CoV-2 GFP/ Δ N trVLP at
309 a MOI of 0.05. After 2 days, GFP fluorescence was determined (**Fig.6 B-E**). Remdesivir
310 and GC376 exhibited potent antiviral effect with IC_{50} =62.5 nM and 4.5 μ M respectively,
311 with essentially no apparent cytotoxic effect (**Fig.6 B and C**). In contrast, Lopinavir or
312 ritonavir inhibited SARS-CoV-2 GFP/ Δ N trVLP with IC_{50} =8.7 μ M, or 7.7 μ M, while
313 those drugs both show serious cytotoxicity at the IC_{50} concentration (**Fig.6 D and E**),
314 compromising their clinical utilities, which is in line with the fact that lopinavir and
315 ritonavir as no significant beneficial effect was observed in a randomized trial
316 established in March 2020 with a total of 1,596 patients³⁴.

317 These results demonstrated that our experimental system can be used for
318 evaluation of antivirals and could be potentially developed for high-throughput
319 screening of antiviral compounds.

320 **Identification of potent antivirals against SARS-CoV-2 virus using trVLP cell** 321 **culture model by high-throughput screening**

322 To provide proof-of-concept that our system could be utilized in high-throughput
323 screening, we performed HTS of Topscience natural product library containing 377
324 drugs (**Fig. 7A**) and the potential hit compounds were further assessed using authentic

325 SARS-CoV-2 to confirm the antiviral activities *in vitro*. DMSO or remdesivir were
326 included as the negative or positive control.

327 Among the 377 compounds of the compound library, 10 hit molecules showed
328 equal or higher inhibition with an inhibitory efficiency $\geq 60\%$ (**Fig. 7A**). In addition,
329 we excluded five hits due to the visible cytotoxicity. This criterion allowed the selection
330 of five hits as the highest confident hits: salinomycin, tubeimoside I, monensin sodium,
331 lycorine chloride and nigericin sodium (**Fig. 7A**). Among these five compounds,
332 lycorine chloride, salinomycin and monensin sodium inhibit HCoV-OC43 infection as
333 previously reported³⁵ and monensin sodium blocks avian infectious bronchitis virus
334 (IBV) infection³⁶. Notably, a recent study demonstrated that salinomycin possessed a
335 potent antiviral activity to inhibit SARS-CoV-2 infection *in vitro*³⁷, which further
336 demonstrated that our system could be used for HTP antiviral screening. We next
337 determined the IC₅₀ of the hit compounds using authentic SARS-CoV-2 virus.
338 Salinomycin showed SARS-CoV-2 antiviral activity with an IC₅₀ and CC₅₀ of 2.836
339 and 20.23 μM , respectively, and selectivity index (SI = CC₅₀/IC₅₀) of 7.13. In
340 comparison, other four compounds did not show dramatic cytotoxic effect in the tested
341 concentrations. Of note, tubeimoside I exhibited an IC₅₀ of 1.371 μM ; monensin sodium
342 exhibited an IC₅₀ of 0.632 μM ; lycorine chloride showed antiviral activity with an IC₅₀
343 of 0.773 μM , and nigericin sodium, exhibited an IC₅₀ of 11.25 μM . These results
344 demonstrated that the compounds we identified using SARS-CoV-2 GFP/ ΔN trVLP
345 system exhibited potent antiviral activity against authentic SARS-CoV-2 infection, and
346 our screening provided new candidate compounds to effectively treat infection of
347 SARS-CoV-2.

348

349

350 **DISCUSSION**

351 As its high pathogenicity and the lack of effective vaccines and therapeutics,
352 SARS-CoV-2 is classified as a biological safety level 3 (BSL-3) pathogen³⁸, which has
353 hindered the drug discovery and biological research due to biocontainment
354 requirements. In this study, we developed an *in vitro* cell culture system to produce the
355 recombinant SARS-CoV-2 virus lacking the N-encoding region in the viral genome
356 (SARS-CoV-2 Δ N). Recombinant SARS-CoV-2 Δ N can expand and propagate in
357 packaging cells (Caco-2-N) but results in only single-cycle infection in naïve Vero or
358 Caco-2 cells, which biologically contained the virus in the cells expressing N protein.
359 This BSL-2 SARS-CoV-2 possesses a reporter gene GFP, providing a surrogate readout
360 for authentic viral infection. We monitored the recombinant virus infection in the Caco-
361 2-N cells for one month and NGS sequencing result suggested that no recombination
362 was detected. In addition, we utilized the split intein-mediated protein ligation to
363 reconstitute N function which further ensure the biosafety of this system.

364 This cell model represents a unique system in the basic research application for
365 better understanding SARS-CoV-2 life cycle. Virus has evolved since its outbreak in
366 the end of last year, and some mutations or deletions have been observed. However, the
367 functional consequences of these mutations or deletions on virus infectivity or
368 pathogenesis is poorly characterized. Herein, we utilized our model system to study the
369 roles of N in the SARS-CoV-2 life cycle. Since N can be expressed alone *in trans*, it is
370 convenient to perform mutagenesis on N to dissect its detailed function. Moreover, the
371 introduction of mutations *in trans*-expressed N will avoid the cis effects of the
372 mutations, for example, the disruption of critical RNA secondary or tertiary structures
373 in the SARS-CoV-2 genome, thereby providing a more appropriate system to
374 specifically evaluate the biological roles of domains, motifs, or amino acid residues
375 within the N protein. Additionally, we inserted a Flag tag at the C terminus of N, which
376 did not impair the ability of N to rescue viral production. With this Flag tag, N can be
377 detected and immunoprecipitated by an anti-FLAG antibody (**Fig. S4A**). Multiple
378 amino acids in N protein can be phosphorylated, but our data demonstrated that most

379 of these phosphorylation may not be required for N function at least *in vitro*. Meanwhile,
380 we also identified numerous host factors associated with N protein (**Fig. S4A; Table**
381 **S2**), notably, we also found that N protein could interact with G3BP1 and G3BP2, the
382 stress granule assembly proteins, which was in line with previous studies^{39,40}. Recent
383 studies found that N protein could impair the stress granule assembly to escape the
384 antiviral effect^{40,41}. Thus, the trVLP system provides a new tool to study host factors
385 and viral proteins that may interact with N during SARS-CoV-2 infection.

386 Development of effective therapeutics for COVID-19 remains an urgently unmet
387 medical need. This recombinant trVLP recapitulates the complete SARS-CoV-2 life-
388 cycle in the Caco-2-N or Caco-2-N^{intein} cells. The reporter readout of the virus, such as
389 fluorescent proteins or luminescent proteins, offers a rapid, real-time, quantitative and
390 less labor-intensive measures than traditional methods of viral titer reduction.
391 Importantly, the reporter virus-based assay could cooperate with a BSL-2 compatible
392 high-content screening platform to facilitate antiviral screening. Thus, we developed a
393 96-well format to screen the antiviral compounds in the Topscience Natural Compounds
394 Library, and we identified five compounds which could efficiently block SARS-CoV-2
395 infection. Among them, lycorine, salinomycin and monensin have been reported as the
396 potent inhibitors against HCoV-OC43 infection³⁵, and salinomycin could block SARS-
397 CoV-2 infection as reported recently³⁷. Those data further validate the suitability of our
398 trVLP system in drug discovery. In our screening, we identified Tubeimoside I and
399 nigericin sodium as novel compounds which exhibited potent antiviral activities against
400 authentic SARS-CoV-2 infection *in vitro*. Future studies could be performed to evaluate
401 their antiviral activities *in vivo*.

402 Additionally, there is an urgently need for effective vaccines to contain SARS-
403 CoV-2 pandemic³⁸. The recombinant SARS-CoV-2 lacking of N gene should provide a
404 new means of vaccine development. The greatest advantage of SARS-CoV-2 Δ N is that
405 this virus possesses all the structural viral proteins to induce humoral immune responses
406 and that, upon infection, it could produce all the nonstructural viral proteins in host cells
407 to induce cell-mediated immune responses. Of course, further studies, especially in

408 animals, are needed to determine the immunogenicity, safety, and efficacy of it.

409 In summary, the biologically contained SARS-CoV-2 trVLP lacking the N gene
410 represents a safe, alternative experimental system to study SARS-CoV-2 biology and
411 to screen antiviral compounds and this novel system will greatly accelerate current
412 SARS-CoV-2 research efforts.
413

414 **ACKNOWLEDGEMENTS**

415 We thank Di Qu, Xia Cai, Zhiping Sun, Wendong Han, and other colleagues at
416 the Biosafety Level 3 Laboratory of Fudan University for help with experiment design
417 and technical assistance. We thank Dr. Guocai Zhong (Shenzhen Bay Laboratory,
418 Shenzhen, China) for generously providing the recombinant ACE2-Fc protein. We
419 thank Prof. Haiteng Deng and Xianbin Meng in Proteinomics Facility at Technology
420 Center for Protein Sciences, Tsinghua University, for protein MS analysis. We thank
421 Dr. Jenna M. Gaska for suggestions and revision of the manuscript. We are grateful to
422 other members of the Ding lab for critical discussions and comments on the
423 manuscript.

424 This work was supported by Tsinghua-Peking University Center of Life Sciences
425 (045-61020100120), Tsinghua University Initiative Scientific Research Program
426 (2019Z06QCX10), National Natural Science Foundation of China (32041005),
427 National Key Research and Development Program of China (2020YFA0707701),
428 Beijing Advanced Innovation Center for Structure Biology (100300001), Start-up
429 Foundation of Tsinghua University (53332101319), Project of Novel Coronavirus
430 Research of Fudan University (to Y.X.), and Development Programs for COVID-19 of
431 Shanghai Science and Technology Commission (20431900401).

432 **Potential Competing Interest statements**

433 Q.D. and X.J. have filed a patent application on the use of the SARS-CoV-2
434 transcomplementation system and its use for anti-SARS-CoV-2 drug screening.

435
436

437

438 **MATERIALS And METHODS**

439 **Cell culture.** HEK293T, Vero, Vero E6, A549 and Caco-2 cells were maintained in
440 Dulbecco's modified Eagle medium (DMEM) (Gibco, China) supplemented with 10%
441 (vol/vol) fetal bovine serum (FBS), and 50 IU/ml penicillin/streptomycin in a
442 humidified 5% (vol/vol) CO₂ incubator at 37°C. All cell lines were tested negative for
443 mycoplasma.

444 **Cloning of the SARS-CoV-2-GFP/ Δ N cDNA.** cDNAs (Wuhan-Hu-1, MN908947) of
445 SARS-CoV-2-GFP/ Δ N were synthesized from the GenScript company. PCR was
446 conducted to amplify fragments A, B, C, D and E using high fidelity PrimeSTAR Max
447 DNA Polymerase (Takara). T7 promoter was introduced upstream of 5' UTR of SARS-
448 CoV-2 genome in fragment A. To guarantee a seamless assembly of the full-length
449 cDNA, type IIS restriction endonuclease sites (BsaI or BsmBI) were introduced at both
450 ends of PCR fragments. The primers used for the PCR assay were listed in
451 Supplemental Table 1.

452 **Assembly of a Full-Length SARS-CoV-2-GFP/ Δ N cDNA.** PCR fragments were
453 digested with BsaI or BsmBI restriction enzyme (NEB) to specific sticky end. Digested
454 fragments are purified by E.Z.N.A gel extraction kit (Omega). Fragment A, B are
455 ligated first by T4 DNA ligase (NEB) in 40 μ l system. At the same time, fragments C,
456 D, E are also ligated in another tube at 4°C for 24 hours. Then, fragment A, B and C,
457 D, E are combined together added with 2 μ l T4 DNA ligase buffer and 2 μ l T4 DNA
458 ligase to 100 μ l at 4°C for another 24 hours. At the end of ligation, we took 5 μ l product
459 to run an agarose gel to check the efficiency of ligation. Full-length assembly cDNA
460 was phenol/chloroform extracted, isopropanol precipitated, and resuspended in 10 μ L
461 nuclease-free water.

462 **RNA *in vitro* transcription, electroporation and virus production.** RNA transcript
463 was *in vitro* transcribed by the mMMESSAGE mMACHINE T7 Transcription Kit
464 (ThermoFisher Scientific) in 30 μ l system with some modifications. Twenty
465 micrograms of viral RNA and 20 μ g N mRNA were mixed and added to a 4-mm cuvette

466 containing 0.4 mL of Caco-2-N cells (8×10^6) in Opti-MEM. Single electrical pulse was
467 given with a GenePulser apparatus (Bio-Rad) with setting of 270V at 950 μ F. GFP signal
468 can be observed 17 hours post electroporation. Three days post electroporation, P0 virus
469 was collected and Caco-2-N cells were infected with P0 virus to amplify virus.

470 **Lentivirus packaging.** Vesicular stomatitis virus G protein (VSV-G) pseudotyped
471 lentiviruses were produced by transient cotransfection of the third-generation
472 packaging plasmids pMD2G (catalog no. 12259; Addgene), psPAX2 (catalog number
473 12260; Addgene) and the transfer vector pLVX by VigoFect DNA transfection reagent
474 (Vigorous) into HEK293T cells. The medium was changed 12 h post transfection.
475 Supernatants were collected at 36, 60 and 84 h after transfection, pooled, passed
476 through a 0.45- μ m filter, aliquoted, and frozen at -80°C refrigerator.

477 **RNA isolation and RT-qPCR.** Total cellular RNA was isolated using TRNzol reagent
478 (Thermo, 15596018). To analyze the RNA level of SARS-CoV-2 in infected cells,
479 quantitative real-time PCR was performed. In brief, 1 μ g total RNA was reverse
480 transcribed using ReverTra Ace qPCR RT Kit (TOYOBO, FSQ-101) to produce cDNA
481 with random primers. Reactions of qPCR were carried out using the 2 \times RealStar Green
482 Power Mixture (Genstar, A311) according to the instruction. The qPCR primers for
483 viral RNA were as follows: THU-2190 (5'- CGAAAGGTAAGATGGAGAGCC-3')
484 and THU-2191 (5'- TGTTGACGTGCCTCTGATAAG-3'). The sequences of the qPCR
485 primers for GAPDH was described previously⁴². Relative expression levels of the target
486 genes were calculated using the comparative cycle threshold (CT) method. All data
487 were normalized relative to the housekeeping gene GAPDH.

488 **RNA-seq and data analysis.** Total RNA was extracted by using TRIzol™ Reagent
489 (Invitrogen) according to the manufacturer's protocol. The rRNAs were removed by
490 using Ribo-Zero Gold module of Illumina TruSeq stranded total RNA library prep kit
491 (RS-122-2201) and then cDNA libraries were constructed according to the
492 manufacturer's protocol. RNA-seq was performed by using the Illumina Novaseq
493 platform. The reference genome of SARS2 (MN908947) was downloaded from
494 <https://www.ncbi.nlm.nih.gov/nuccore/MN908947>. After removing low-quality

495 reads, remaining Illumina sequence reads were mapped to human (GRCh38) and
496 SARS2 genome by using HISAT2.1.0 with parameters: --rna-strandness RF -dta.
497 RNA-seq coverage was visualized by using Integrative Genomics Viewer (IGV). To
498 quantify the expression levels of SARS2 genes, RPKM of each virus genes and GFP
499 gene were calculated. Heatmaps were drawn by using R package “pheatmap”
500 (<https://www.r-project.org>). To quantify the junction-reads from subgenomic RNAs,
501 the STAR2.7.5c was used for reads mapping. The junction-reads was defined and
502 collected as described in Kim, Cell, 2020. A Sankey diagram was drawn by using R
503 packages named “networkD3” and “dplyr”.

504 **IFN- β , neutralizing antibody and drug treatment.** To assess the antiviral efficacies
505 of the materials, 1×10^4 Caco-2-N cells were seeded into 96-well plates. After 12h, cells
506 were infected with SARS-CoV-2-GFP Δ N virus at MOI of 0.05. For neutralizing
507 antibody treatment, virus was incubated with neutralizing antibody for 1 hour at 37°C
508 before infection. For IFN- β (Sino Biological, 10704-HNAS-5) test, cells were pre-
509 treated with IFN- β for 8 hours before infection. For remdesivir (MedChemExpress,
510 HY-104077), lopinavir (biochempartner, BCP01395) or ritonavir (biochempartner,
511 BCP03777) treatment, drugs were added simultaneously upon infection. Two days after
512 infection, flow cytometry was performed to analyze GFP positive rate. The 50%
513 inhibitory concentrations (IC50; compound concentration required to inhibit viral
514 replication by 50% reduction of GFP positive cells) were determined using logarithmic
515 interpolation using GraphPad Prism software version 7.0.

516 **Cell viability assay.** Caco-2-N cells were seeded into 96-well plate (1×10^3 cells/well).
517 After 12 hours, cells were treated with drugs with different concentrations. Cell
518 viability was measured two days post treatment with CellTiter-Glo Luminescent Cell
519 Viability Assay kit (Promega, G7570) following standard protocol. In brief, cells in 100
520 μ l culture medium were added with 100 μ l CellTiter-Glo reagent. After 15 minutes,
521 luminescence was recorded with GloMax (Promega). CC₅₀ was determined using
522 logarithmic interpolation using GraphPad Prism software version 7.0.

523 **Flow cytometry analysis.** Cells were detached in PBS containing 0.02% EDTA and

524 then washed once with cold PBS. Cells were then fixed in 4% PFA for 30 minutes at
525 room temperature. Fixed cells were resuspended in PBS and analyzed by LSRFortessa
526 SORP (BD Biosciences) and FlowJo software.

527 **Western blotting.** Sodium dodecyl sulfate-polyacrylamide gel electrophoresis (SDS-
528 PAGE) immunoblotting was conducted as follows: After trypsinization and cell
529 pelleting at 1500 r/m for 10 min, whole-cell lysates were harvested in cell lysis buffer
530 (50 mM Tris-HCl [pH 7.5], 150mM NaCl, 1% NP-40, 1mM EDTA) supplemented with
531 protease inhibitor cocktail (Sigma). Lysates were electrophoresed in 4-12%
532 polyacrylamide gels and transferred onto PVDF membrane. The blots were blocked at
533 room temperature for 0.5 h using 5% nonfat milk in 1× phosphate-buffered saline (PBS)
534 containing 0.1% (v/v) Tween 20. The blots were exposed to primary antibodies anti-N
535 (05-0154, AbMax), S (40589-T62, Sino Biological), β-Tubulin (CW0098, CWBIO),
536 Flag (F7425, Sigma), ACE2 (10108-T24, Sino Biological) in 5% nonfat milk in 1×PBS
537 containing 0.1% Tween 20 for 2 h. The blots were then washed in 1×PBS containing
538 0.1% Tween 20. After 1h exposure to HRP-conjugated secondary antibodies and
539 subsequent washes were performed as described for the primary antibodies.
540 Membranes were visualized using the Luminescent image analyzer (GE).

541 **Antiviral screening.** Twelve hours prior to infection for the antiviral screening 5×10^4
542 Caco-2-N^{int} cells were seeded in 96 well plates. The next day, a single dilution of each
543 compound of the Topscience Natural Product Library at 5 μM final concentration was
544 added to the cells (50 μL/well). DMSO or remdesivir (3.5μM) were included in each
545 plate as the internal control. After 2 hours, 50 μL of virus was added to the wells at MOI
546 0.05. Two days after infection, cells were collected for flow cytometry analysis to
547 determine the GFP expression.

548 **Evaluation of antiviral activity using authentic SARS-CoV-2 virus.** A549 cells
549 stably expressing human ACE2 were seeded in a 96-well plate (4×10^4 cells/well). Next
550 day, cells were treated with drugs (Lycorine chloride (TargetMol, T2774), Tubeimoside
551 I (TargetMol, T2715), Nigericin sodium (TargetMol, T3092), Monensin sodium
552 (MedChemExpress, HY-N0150), Salinomycin (MedChemExpress, HY-15597)) of

553 different concentration for 2 hours prior to infection. Cells were infected with SARS-
554 CoV-2 at an MOI of 1 for 1 h, washed three times with PBS, and incubated in 2% FBS
555 culture medium for 24 h for viral antigen staining. Cells were fixed with 4%
556 paraformaldehyde in PBS, permeablized with 0.2% Triton X-100, and incubated with
557 the rabbit polyclonal antibody against SARS-CoV nucleocapsid protein (Rockland,
558 200-401-A50, 1 μ g/ml) at 4 °C overnight. After three washes, cells were incubated with
559 the secondary goat anti-rabbit antibody conjugated with Alexa Fluor 555 (Thermo
560 #A32732, 2 μ g/ml) for 2 h at room temperature, followed by staining with 4',6-
561 diamidino-2-phenylindole (DAPI). Images were collected using an Operetta High
562 Content Imaging System (PerkinElmer). For high content imaging, two biological
563 replicates for each concentration of drug were scanned and five representative fields
564 were selected for each well of 96-well plates. Image analysis was performed using the
565 PerkinElmer Harmony high-content analysis software 4.9. Cells were automatically
566 identified by DAPI (nuclei). Mean fluorescent intensity of channel Alexa 555 (viral
567 nucleocapsid) of each cell were subsequently calculated, respectively. For the 0%
568 inhibition control, cells were infected in the presence of vehicle only. The IC₅₀ value
569 was defined as the concentration at which there was a 50% decrease in N protein
570 expression. Data were analyzed using GraphPad Prism 7.0. The IC₅₀ values were
571 calculated by nonlinear regression analysis using the dose-response (variable slope)
572 equation (four parameter logistic equation).

573 **Statistical analysis.** Student's *t* test or one-way analysis of variance (ANOVA) with
574 Tukey's honestly significant difference (HSD) test was used to test for statistical
575 significance of the differences between the different group parameters. *P* values of less
576 than 0.05 were considered statistically significant.

577 **Data availability.** RNA-seq dataset generated here can be found in the aforementioned
578 NCBI Gene Expression Omnibus (GEO Accession no. GSE162629,
579 <https://www.ncbi.nlm.nih.gov/geo/query/acc.cgi?acc=GSE162629>). Other data from
580 this study are available upon request from the corresponding author.

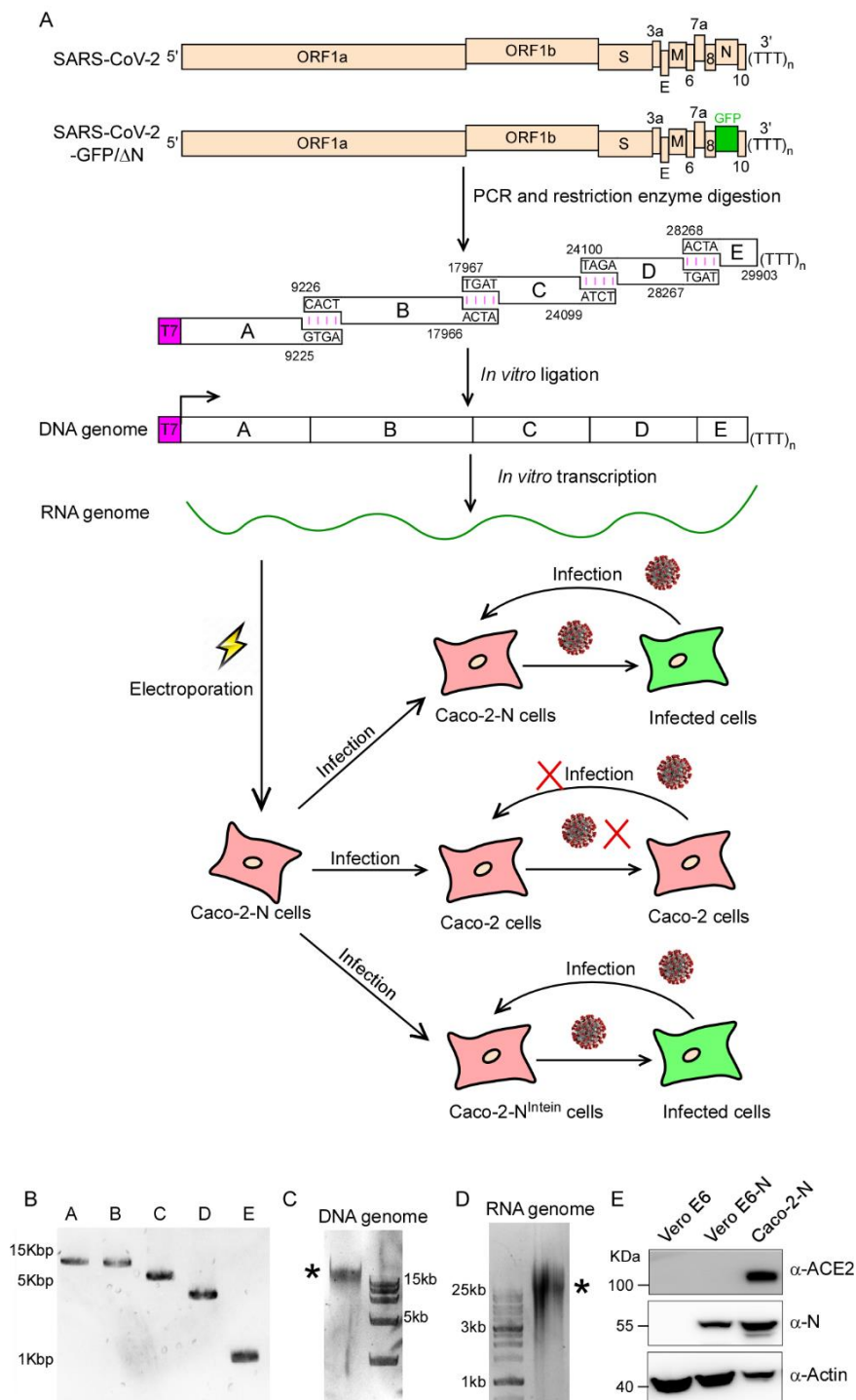
581

582

583 FIGURES AND FIGURE LEGENDS

584

Figure 1

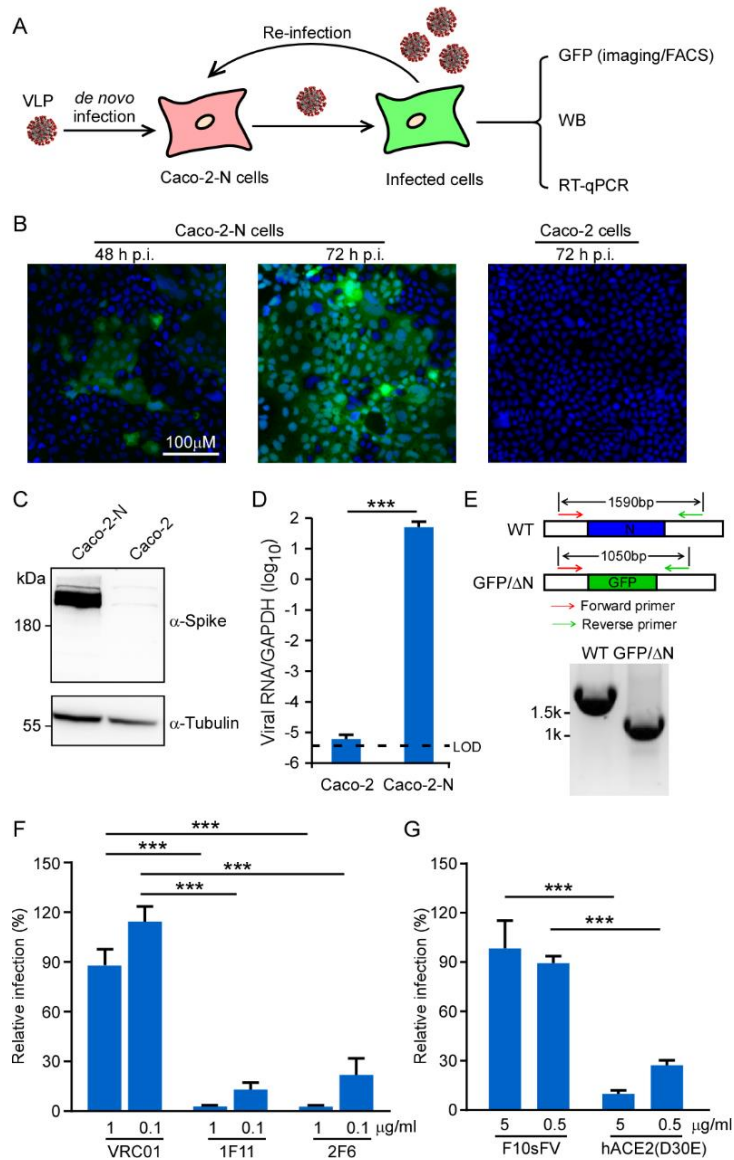


585 **Figure 1. Production of SARS-CoV-2 GFP/ Δ N trVLP.** (A) The top rows show
586 genetic organizations of the SARS-CoV-2 and SARS-CoV-2 GFP/ Δ N genomes. The
587 ORF of N is replaced with reporter gene (GFP here). The cDNA of SARS-CoV-2
588 GFP/ Δ N genome was divided into five fragments designated as Fragment A, B, C, D
589 and E, which could be obtained by PCR (B). Each cDNA fragment was flanked by a
590 class IIS restriction endonuclease site (BsaI or BsmBI) and the nucleotide sequences
591 and locations of the cohesive overhangs are indicated. The fragment cDNA were
592 digested and purified for directed assembly of SARS-CoV-2 GFP/ Δ N cDNA (see C
593 panel, and the star indicates the genome-length cDNA), which served as the template
594 for *in vitro* transcription to generate viral RNA genome (see D panel, and the star
595 indicates the genome-length RNA transcript). The viral genomic RNAs were
596 electroporated into Caco-2-N cells. After 3 days, the supernatant was collected and
597 inoculated with Caco-2 or Caco-2-N cells. (E). Western blotting assay was performed
598 to detect the expression of N proteins and ACE2 in Caco-2-N cells, Vero E6 and Vero
599 E6-N cells.

600
601

602

Figure 2



603

604 **Figure 2. The recombinant SARS-CoV-2 GFP/ΔN trVLP can propagate with the**
 605 **help of viral N protein.** (A) Experimental scheme. Caco-2 or Caco-2-N cells were
 606 infected with SARS-CoV-2 GFP/ΔN for 3h (MOI 0.05), washed, and incubated for an
 607 additional 72 h. GFP fluorescence were observed or quantified by microscopy or flow
 608 cytometry analysis. Viral RNA was determined by RT-qPCR assay; (B) GFP
 609 expression was observed in Caco-2 or Caco-2-N cells using microscopy at indicated
 610 time point after inoculation; Representative images from one of three independent

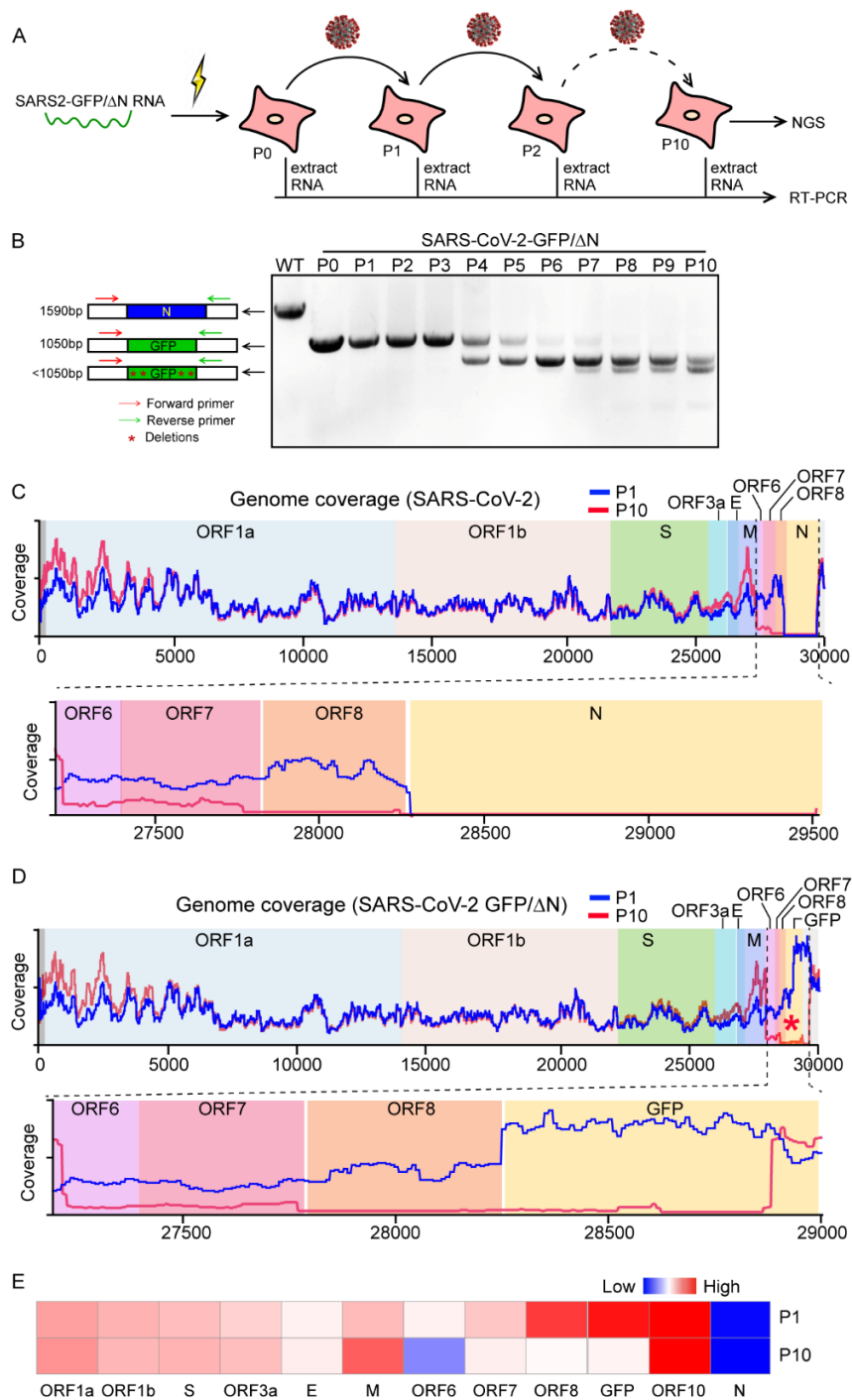
611 experiments. (C) Cell lysates were resolved by SDS-PAGE and probed with anti-
612 Spike and anti-Tubulin antibodies. Representative images from two independent
613 experiments; (D) The total RNAs were extracted and RT-qPCR assays were
614 conducted to determine viral RNA levels. Error bars represent the standard deviations
615 from one of two independent experiments performed in triplicate; (E) RT-PCR
616 analysis of the SARS-CoV-2 GFP/ Δ N genome in Caco-2-N cells infected with
617 recombinant virus using a primer set flanking the N region. The expected DNA sized
618 were indicated in each genome, and DNA marker is shown on the left. Representative
619 images from one of two independent experiments; (F-G) Recombinant SARS-CoV-2
620 GFP/ Δ N virus was incubated with indicated doses of neutralizing mAbs against
621 SARS-CoV-2 (1F11 and 2F6) or HIV (VCR01), as well as soluble human ACE2-Fc or
622 F10sFV for 1 h prior to inoculation. The infection was analyzed by GFP expression 2
623 days later, and the number of positive cells was expressed as a percentage of that for
624 the VRC01 or F10sFV treatment control. Error bars represent the standard deviations
625 from three independent experiments (n=6). ***, $P < 0.001$. Significance assessed by
626 one-way ANOVA.

627

628

629

Figure 3



630 **Figure 3. Characterization of the genetic stability of SARS-CoV-2 GFP/ΔN trVLP.**
 631 (A) Detection of the GFP reporter gene during viral passage. RNAs were extracted from
 632 the VLP infected cells of P0 to P10 passage, respectively. (B) RT-PCR was performed

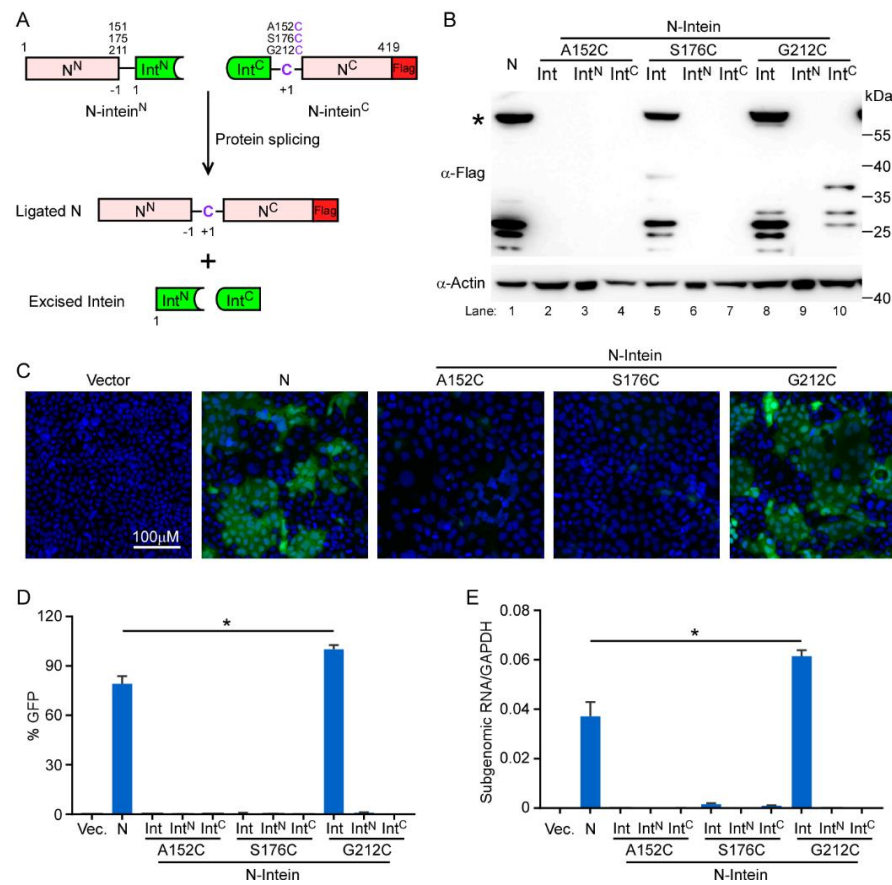
633 with a primer pair flanking the N region of ORF8 and 3'UTR. The PCR products were
634 resolved on an agarose gel using electrophoresis. The numbers of time points-samples-
635 passage were denoted on the top of each lane. Representative images from one of three
636 independent experiments; (C-D) RNA-seq coverage of viruse derived reads aligned to
637 SARS-CoV-2 (C) or SARS-CoV-2 GFP/ Δ N (D) genome, respectively. (E) Heatmap
638 shows the expression levels of each subgenomic RNA of P1 or P10 trVLP.

639

640

641

Figure 4

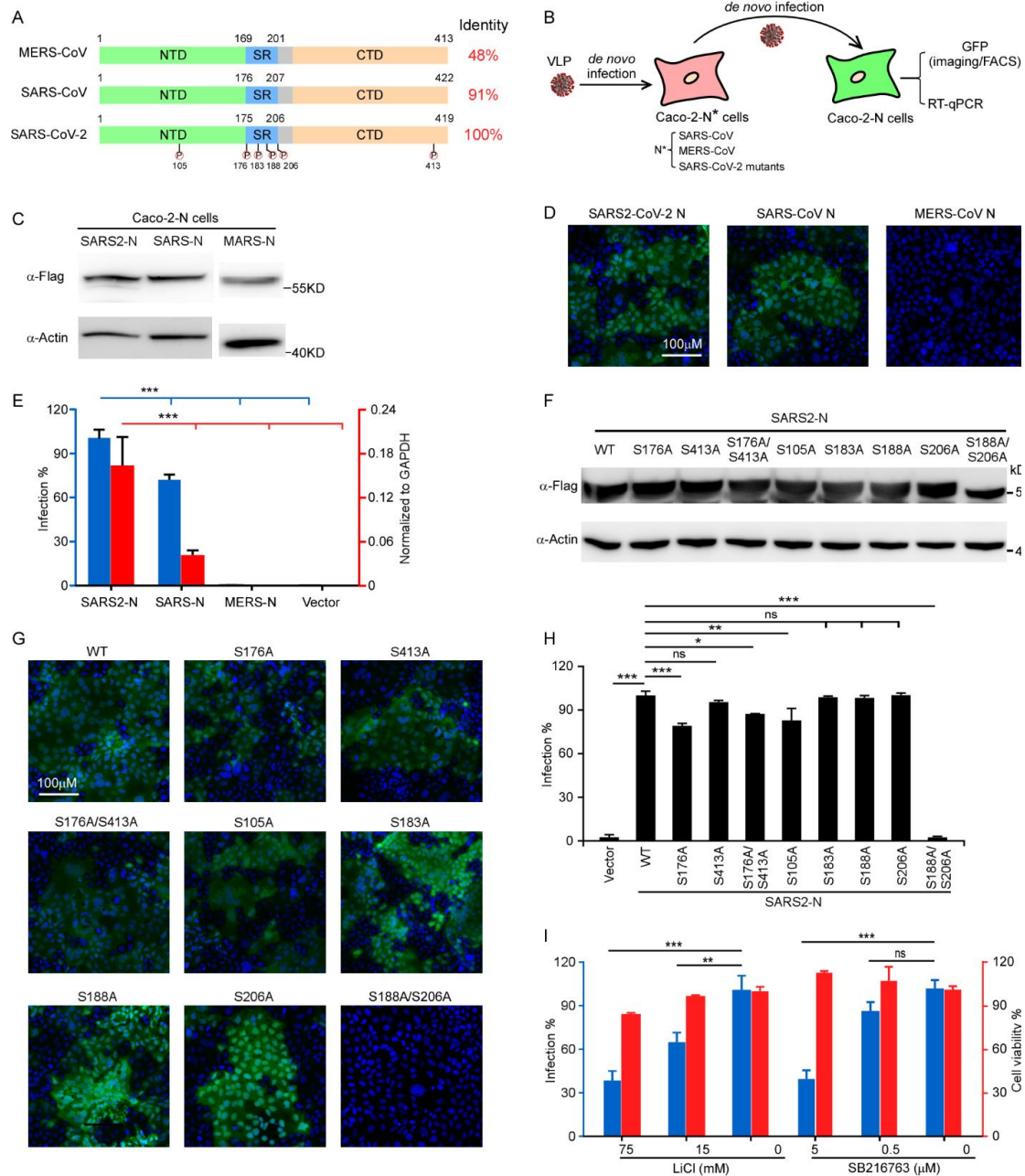


642 **Figure 4. Reconstitution of functional N protein by intein-mediated protein**
 643 **splicing.** (A) Scheme depicting of intein-mediated protein trans-splicing to reconstitute
 644 full length N protein. (B) Western blot (WB) analysis of lysates from Caco-2 cells
 645 transduced with either full-length N or intein-N lentiviruses. The star indicates the full-
 646 length N protein. The WB is representative of three independent experiments. (C) GFP
 647 fluorescence in Caco-2-N cells infected cell culture medium (containing SARS-CoV-2
 648 GFP/ΔN progeny) collected from each Caco-2-N^{int} cells which was inoculated with
 649 SARS-CoV-2 GFP/ΔN trVLP at 2 days of culture. The image is representative of n=4.
 650 (D) Cells were harvested to quantify GFP expression by flow cytometry analysis, and
 651 (E) Subgenomic RNA of E were determined by RT-qPCR assay. Error bars represent
 652 the standard deviations from one of three independent experiments performed in
 653 triplicate. *, P < 0.05. Significance assessed by one-way ANOVA.

654

655

Figure 5



656 **Figure 5. Site-specific phosphorylation of N is required to support virus life cycle.**

657 (A) Schematics and alignments of N proteins from MERS-CoV, SARS-CoV and SARS-

658 CoV-2. The phosphorylation sites in SARS-CoV-2 N protein were highlighted. (B)

659 Schematic presentation of assessment of N variants function. The trVLP inoculated

660 with Caco-2 cells transduced with N variants, and the cell culture medium were

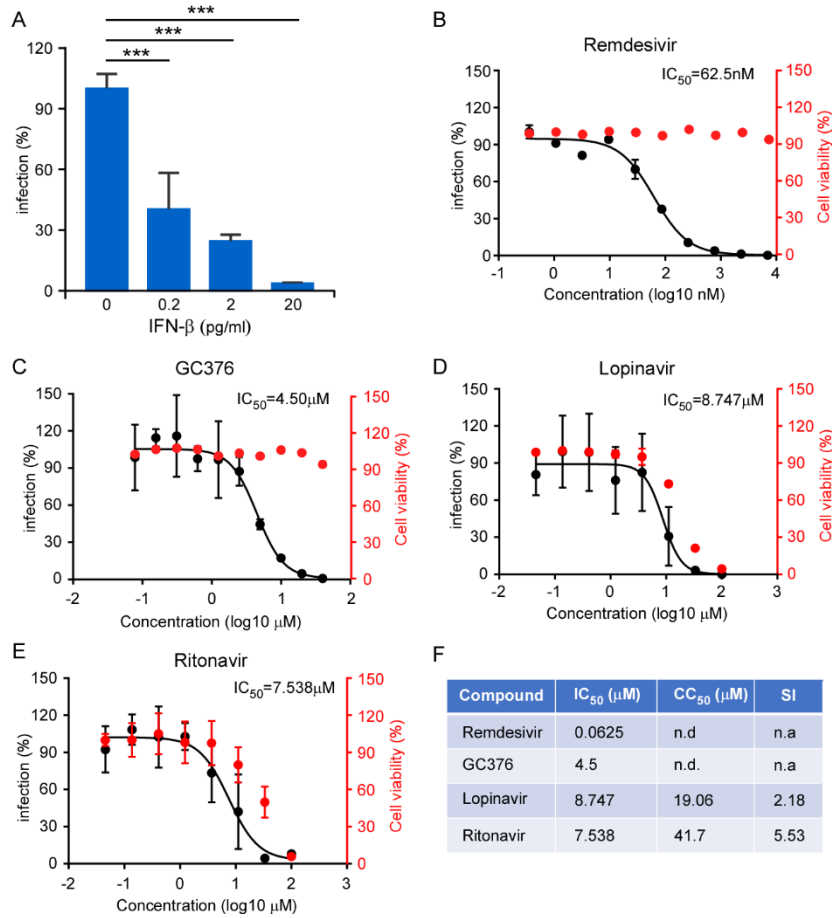
661 collected to infect the Caco-2-N cells, and GFP expression analyzed by flow
662 cytometry/microscopy or viral subgenomic RNA abundance were determined by RT-
663 qPCR. (C) Western blotting assay was performed to detect the N proteins expression in
664 Caco-2 cells transduced with distinct N genes from SARS-CoV-2, SARS-CoV or
665 MERS-CoV. (D-E) The cell culture medium was collected from SARS-CoV-2 GFP/ Δ N
666 trVLP infected Caco-2 cells expressing N from SARS-CoV-2, SARS-CoV or MERS-
667 CoV to infect the naïve Caco-2-N cells. GFP were observed using microscopy and
668 cellular RNA was extracted for RT-qPCR analysis to determine viral subgenomic RNA
669 levels. (F) Western blotting assay detected the expression of SARS-CoV-2 N WT or
670 mutants in Caco-2 cells. (G-H) The cell culture medium was collected from SARS-
671 CoV-2 GFP/ Δ N trVLP infected Caco-2 cells expressing SARS-CoV-2 N mutants to
672 infect the naïve Caco-2-N cells. GFP were observed using microscopy and cellular
673 RNA was extracted for RT-qPCR analysis to determine viral subgenomic RNA levels.
674 (I) GSK-3 inhibitors LiCl or SB216763 treated Caco-2-N cells inoculated with SARS-
675 CoV-2 GFP/ Δ N trVLP, the cell culture medium was then inoculated with Caco-2-N
676 cells. RNA was extracted for RT-qPCR analysis to determine viral subgenomic RNA
677 levels. Cell viability was evaluated by CellTiter-Glo assay. Error bars (E, H and I)
678 represent the standard deviations from one of three independent experiments performed
679 in triplicate. n.s. no significance; *, $P < 0.05$; **, $P < 0.01$; ***, $P < 0.001$. Significance
680 assessed by one-way ANOVA.

681

682

683

Figure 6



684 **Figure 6. Inhibition of recombinant SARS-CoV-2 GFP/ΔN trVLP infection by IFN**
 685 **and antivirals.** (A) IFN-β pretreated Caco-2-N^{int} cells were subsequently infected with
 686 trVLP and cells were subjected to flow cytometry analysis for quantify the GFP
 687 fluorescence at 2 days post-infection. Error bars represent the standard deviations from
 688 three independent experiments (n=6). (B-E) Antiviral effect of remdesivir, GC376,
 689 lopinavir and ritonavir. The drug treated cells were infected with trVLP and GFP
 690 fluorescence was quantified at 48h after infection. The cytotoxic effect of each drug at
 691 indicated concentrations were determined by CellTiter-Glo cell viability assay. The
 692 virus infection or cytotoxicity is plotted versus compound concentration (n=3 biological
 693 replicates for all compounds). The black dots indicate replicate measurements, and the

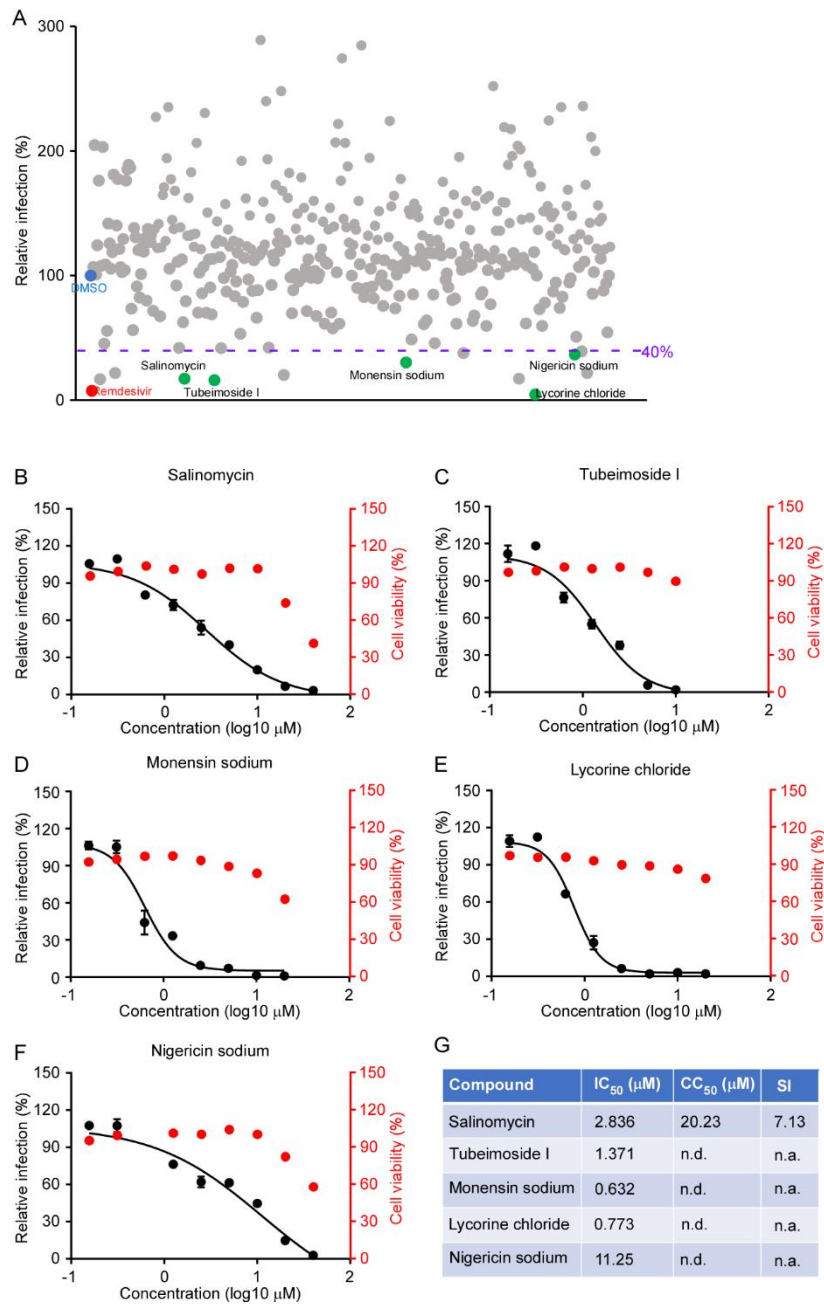
694 black lines indicate dose-response curve fits. The red dots indicate cytotoxicity. IC_{50}
695 values were calculated using Prism software and is representative of one of three
696 independent experiments performed in triplicate. Three independent experiments had
697 similar results. (F) Comparison of antiviral activity and cytotoxicity of each compound.
698 Selectivity Index (SI), a ratio that compares a drug's cytotoxicity and antiviral activity
699 was also calculated. n.d.=not detected; n.a.=not applicable.

700

701

702

Figure 7



703

704 **Figure 7. High throughput screening of antivirals against SARS-CoV-2 infection**

705 **using trVLP system.** (A) Screening of 377 compounds from Topscience Natural

706 Product Library and hits selection. The purple dot line represents the threshold (40%)

707 for positive hit compounds. DMSO (blue) and remdesivir (red) are used as the control

708 for the screening. Each dot represents a single compound, and the green dots represent
709 the promising candidates which exhibited potent antiviral activity without dramatic
710 cytotoxic effect. (B-F) Dose response curves of selected hit compounds. Compounds
711 concentrations are presented in log scale for logarithmic interpolation. Dose response
712 curves were generated using GraphPad Prism software version 7.0. IC_{50} values were
713 calculated using Prism software and is representative of one of three independent
714 experiments. Error bars represent the standard deviations from one of three independent
715 experiments performed in triplicate. (G) Comparison of antiviral activity and
716 cytotoxicity of each compound. Selectivity Index (SI), a ratio that compares a drug's
717 cytotoxicity and antiviral activity was also calculated. n.d.=not detected; n.a.=not
718 applicable.

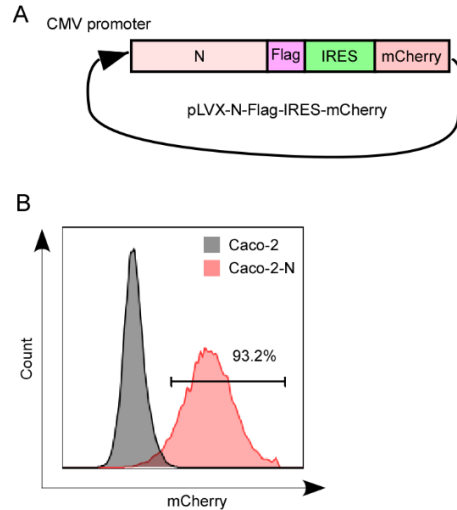
719

720

721 **SUPPLEMENTAL FIGURES AND FIGURE LEGENDS**

722

Fig S1



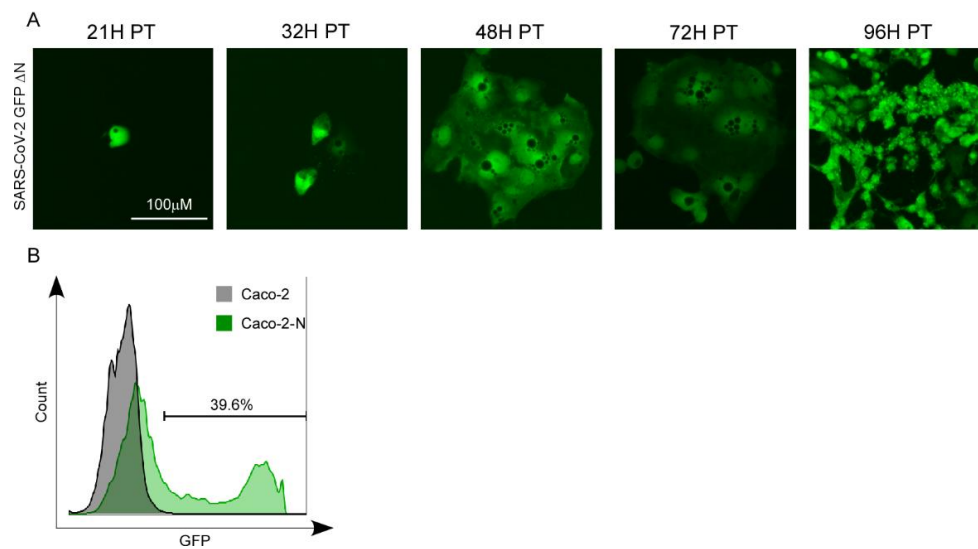
723 **Supplemental Figure 1. Generation of Caco-2 cell expressing SARS-CoV-2 N by**
724 **lentiviral transduction.** (A) Scheme depicting the bicistronic lentiviral constructs for
725 expressing SARS-CoV-2 N protein with C-terminal Flag tag. (B) Representative flow
726 cytometry plots demonstrating efficient lentivirus transduction. Caco-2 cells were
727 transduced with pLVX-N-Flag-IRES-mCherry or not transduced. Flow cytometric
728 analysis was performed 4 d following transduction to quantify the frequencies of N-
729 expressing cells. The flow cytometry result was representative of one of three
730 independent experiments.

731

732

733

Fig S2



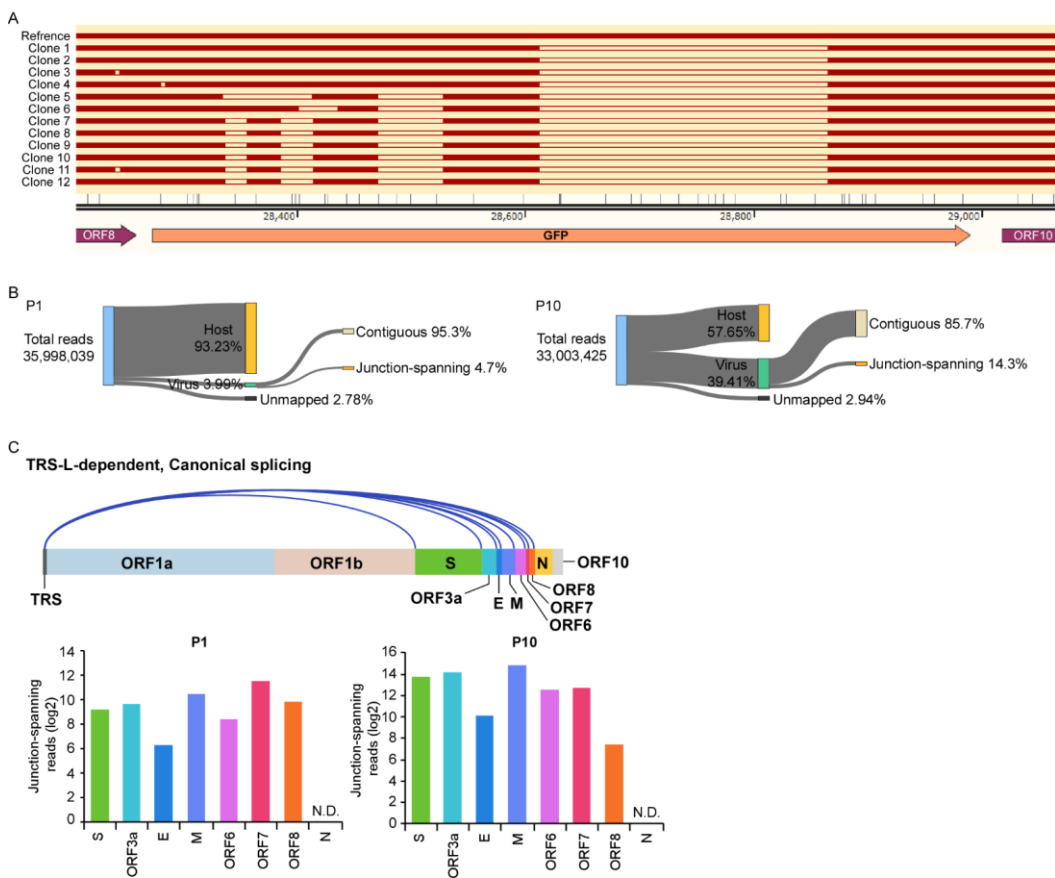
734 **Supplemental Figure 2. GFP expression in Caco-2-N cells electroporated with**
735 **SARS-CoV-2 GFP/ Δ N RNA.** (A) GFP expression in Caco-2-N cells electroporated
736 with SARS-CoV-2 GFP/ Δ N RNA. Caco-2-N cells were electroporated with 20 μ g of
737 SARS-CoV-2 GFP/ Δ N RNA. From 21h-96h p.t., GFP expression in the cells was
738 observed with microscopy. (B) GFP expression was quantified by flowcytometry at 96h
739 post transfection of the RNA. This experiment was representative of three independent
740 experiments.

741

742

743

Fig S3



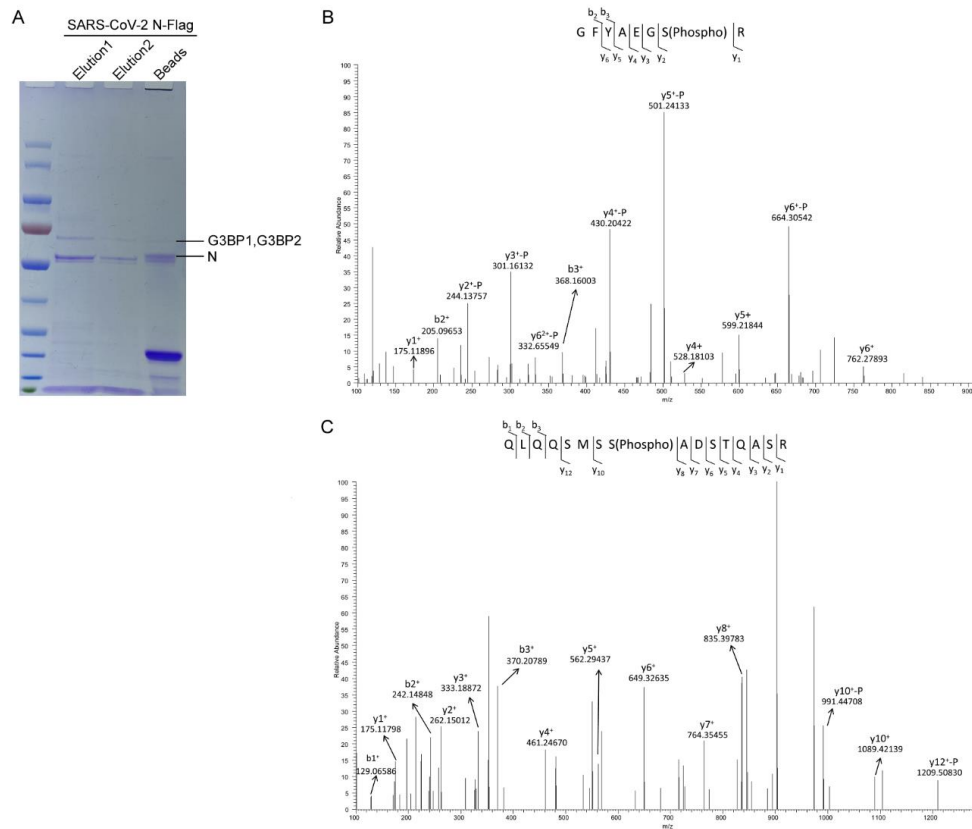
744 **Supplemental Figure 3. Characterization of the genetic stability of SARS-CoV-2**
 745 **GFP/ΔN virus.** (A) RT-PCR products from P10 virus infected cell passage were cloned
 746 into pEASY-Blunt vector, and 12 colonies were randomly chosen for DNA sequences
 747 analysis. Multiple deletions were detected in the amplicon. (B) Categories of mapped
 748 reads from P1 and P10 virus infected Caco-2-N cells. (C) Canonical discontinuous
 749 transcription (top) that is mediated by TRS-L (TRS in the leader) and TRS-B (TRS in
 750 the body). Quantification of junction-reads from canonical discontinuous transcripts
 751 post P1 and P10 virus infection.

752

753

754

Fig S4



755 **Supplemental Figure 4. Identification of host factors associated with N protein and**
 756 **phosphorylation on N protein by mass spectrometry.** (A) Flag tagged N protein was
 757 immunoprecipitated from Caco-2-N cells infected with recombinant SARS-CoV-2
 758 GFP/ Δ N trVLP using Flag antibody, and the proteins were analyzed on SDS-PAGE gel.
 759 The proteins were visualized by Coomassie blue staining. N, G3BP1 and G3BP2 were
 760 labelled. (B) Phosphorylated peptides of N protein derived from Caco-2-N cells. Caco-
 761 2-N cells in which N was C-terminal Flag-tagged were collected and cell lysates were
 762 immunoprecipitated with anti-Flag coupled beads. Phosphorylated peptides of the
 763 immunoprecipitates were analyzed by mass spectrometry.

764

765

766 **REFERENCES**

767

- 768 1 Wang, C., Horby, P. W., Hayden, F. G. & Gao, G. F. A novel coronavirus outbreak of global
769 health concern. *Lancet* **395**, 470-473, doi:10.1016/S0140-6736(20)30185-9 (2020).
- 770 2 Rome, B. N. & Avorn, J. Drug Evaluation during the Covid-19 Pandemic. *N Engl J Med*
771 **382**, 2282-2284, doi:10.1056/NEJMp2009457 (2020).
- 772 3 Fung, T. S. & Liu, D. X. Human Coronavirus: Host-Pathogen Interaction. *Annu Rev*
773 *Microbiol* **73**, 529-557, doi:10.1146/annurev-micro-020518-115759 (2019).
- 774 4 Enjuanes, L., Almazan, F., Sola, I. & Zuniga, S. Biochemical aspects of coronavirus
775 replication and virus-host interaction. *Annu Rev Microbiol* **60**, 211-230,
776 doi:10.1146/annurev.micro.60.080805.142157 (2006).
- 777 5 Lai, M. M. Coronavirus: organization, replication and expression of genome. *Annu Rev*
778 *Microbiol* **44**, 303-333, doi:10.1146/annurev.mi.44.100190.001511 (1990).
- 779 6 Li, F. Structure, Function, and Evolution of Coronavirus Spike Proteins. *Annu Rev Virol* **3**,
780 237-261, doi:10.1146/annurev-virology-110615-042301 (2016).
- 781 7 Zuniga, S. *et al.* Coronavirus nucleocapsid protein facilitates template switching and is
782 required for efficient transcription. *J Virol* **84**, 2169-2175, doi:10.1128/JVI.02011-09 (2010).
- 783 8 Cruz, J. L. *et al.* Coronavirus gene 7 counteracts host defenses and modulates virus
784 virulence. *PLoS Pathog* **7**, e1002090, doi:10.1371/journal.ppat.1002090 (2011).
- 785 9 Liu, D. X., Fung, T. S., Chong, K. K., Shukla, A. & Hilgenfeld, R. Accessory proteins of SARS-
786 CoV and other coronaviruses. *Antiviral Res* **109**, 97-109,
787 doi:10.1016/j.antiviral.2014.06.013 (2014).
- 788 10 Almazan, F. *et al.* Coronavirus reverse genetic systems: infectious clones and replicons.
789 *Virus Res* **189**, 262-270, doi:10.1016/j.virusres.2014.05.026 (2014).
- 790 11 Xie, X. *et al.* An Infectious cDNA Clone of SARS-CoV-2. *Cell Host Microbe* **27**, 841-848
791 e843, doi:10.1016/j.chom.2020.04.004 (2020).
- 792 12 Hou, Y. J. *et al.* SARS-CoV-2 Reverse Genetics Reveals a Variable Infection Gradient in the
793 Respiratory Tract. *Cell* **182**, 429-446 e414, doi:10.1016/j.cell.2020.05.042 (2020).
- 794 13 Ju, B. *et al.* Human neutralizing antibodies elicited by SARS-CoV-2 infection. *Nature* **584**,
795 115-119, doi:10.1038/s41586-020-2380-z (2020).
- 796 14 Zhou, T. *et al.* Structural basis for broad and potent neutralization of HIV-1 by antibody
797 VRC01. *Science* **329**, 811-817, doi:10.1126/science.1192819 (2010).
- 798 15 Chan, K. K. *et al.* Engineering human ACE2 to optimize binding to the spike protein of
799 SARS coronavirus 2. *Science* **369**, 1261-1265, doi:10.1126/science.abc0870 (2020).
- 800 16 Li, Y. *et al.* Potential host range of multiple SARS-like coronaviruses and an improved
801 ACE2-Fc variant that is potent against both SARS-CoV-2 and SARS-CoV-1.
802 doi:10.1101/2020.04.10.032342 (2020).
- 803 17 Quéromès, G. *et al.* Characterization of SARS-CoV-2 ORF6 deletion variants detected in
804 a nosocomial cluster during routine genomic surveillance, Lyon, France. *bioRxiv* (2020).
- 805 18 Addetia, A. *et al.* Identification of multiple large deletions in ORF7a resulting in in-frame
806 gene fusions in clinical SARS-CoV-2 isolates. *J Clin Virol* **129**, 104523,
807 doi:10.1016/j.jcv.2020.104523 (2020).
- 808 19 Riojas, M. A. *et al.* A Rare Deletion in SARS-CoV-2 ORF6 Dramatically Alters the Predicted

- 809 Three-Dimensional Structure of the Resultant Protein. *bioRxiv*,
810 doi:10.1101/2020.06.09.134460 (2020).
- 811 20 Su, Y. C. F. *et al.* Discovery and Genomic Characterization of a 382-Nucleotide Deletion in
812 ORF7b and ORF8 during the Early Evolution of SARS-CoV-2. *mBio* **11**,
813 doi:10.1128/mBio.01610-20 (2020).
- 814 21 Muir, T. W. Semisynthesis of proteins by expressed protein ligation. *Annu Rev Biochem*
815 **72**, 249-289, doi:10.1146/annurev.biochem.72.121801.161900 (2003).
- 816 22 Zettler, J., Schutz, V. & Mootz, H. D. The naturally split Npu DnaE intein exhibits an
817 extraordinarily high rate in the protein trans-splicing reaction. *FEBS Lett* **583**, 909-914,
818 doi:10.1016/j.febslet.2009.02.003 (2009).
- 819 23 Wu, C. H. *et al.* Glycogen synthase kinase-3 regulates the phosphorylation of severe acute
820 respiratory syndrome coronavirus nucleocapsid protein and viral replication. *J Biol Chem*
821 **284**, 5229-5239, doi:10.1074/jbc.M805747200 (2009).
- 822 24 Wu, C. H., Chen, P. J. & Yeh, S. H. Nucleocapsid phosphorylation and RNA helicase DDX1
823 recruitment enables coronavirus transition from discontinuous to continuous transcription.
824 *Cell Host Microbe* **16**, 462-472, doi:10.1016/j.chom.2014.09.009 (2014).
- 825 25 Lokugamage, K. G. *et al.* Type I interferon susceptibility distinguishes SARS-CoV-2 from
826 SARS-CoV. *J Virol*, doi:10.1128/JVI.01410-20 (2020).
- 827 26 Vanderheiden, A. *et al.* Type I and Type III Interferons Restrict SARS-CoV-2 Infection of
828 Human Airway Epithelial Cultures. *J Virol* **94**, doi:10.1128/JVI.00985-20 (2020).
- 829 27 Park, A. & Iwasaki, A. Type I and Type III Interferons - Induction, Signaling, Evasion, and
830 Application to Combat COVID-19. *Cell Host Microbe* **27**, 870-878,
831 doi:10.1016/j.chom.2020.05.008 (2020).
- 832 28 Wang, M. *et al.* Remdesivir and chloroquine effectively inhibit the recently emerged novel
833 coronavirus (2019-nCoV) in vitro. *Cell Res* **30**, 269-271, doi:10.1038/s41422-020-0282-0
834 (2020).
- 835 29 Pruijssers, A. J. *et al.* Remdesivir Inhibits SARS-CoV-2 in Human Lung Cells and Chimeric
836 SARS-CoV Expressing the SARS-CoV-2 RNA Polymerase in Mice. *Cell Rep* **32**, 107940,
837 doi:10.1016/j.celrep.2020.107940 (2020).
- 838 30 Siegel, D. *et al.* Discovery and Synthesis of a Phosphoramidate Prodrug of a Pyrrolo[2,1-
839 f][triazin-4-amino] Adenine C-Nucleoside (GS-5734) for the Treatment of Ebola and
840 Emerging Viruses. *J Med Chem* **60**, 1648-1661, doi:10.1021/acs.jmedchem.6b01594
841 (2017).
- 842 31 Sheahan, T. P. *et al.* Broad-spectrum antiviral GS-5734 inhibits both epidemic and
843 zoonotic coronaviruses. *Sci Transl Med* **9**, doi:10.1126/scitranslmed.aal3653 (2017).
- 844 32 Warren, T. K. *et al.* Therapeutic efficacy of the small molecule GS-5734 against Ebola virus
845 in rhesus monkeys. *Nature* **531**, 381-385, doi:10.1038/nature17180 (2016).
- 846 33 Flexner, C. HIV-protease inhibitors. *N Engl J Med* **338**, 1281-1292,
847 doi:10.1056/NEJM199804303381808 (1998).
- 848 34 Cao, B. *et al.* A Trial of Lopinavir-Ritonavir in Adults Hospitalized with Severe Covid-19. *N*
849 *Engl J Med* **382**, 1787-1799, doi:10.1056/NEJMoa2001282 (2020).
- 850 35 Shen, L. *et al.* High-Throughput Screening and Identification of Potent Broad-Spectrum
851 Inhibitors of Coronaviruses. *J Virol* **93**, doi:10.1128/JVI.00023-19 (2019).
- 852 36 Alonso-Caplen, F. V., Matsuoka, Y., Wilcox, G. E. & Compans, R. W. Replication and

- 853 morphogenesis of avian coronavirus in Vero cells and their inhibition by monensin. *Virus*
854 *Res* **1**, 153-167, doi:10.1016/0168-1702(84)90070-4 (1984).
- 855 37 lanevski, A. *et al.* Potential Antiviral Options against SARS-CoV-2 Infection. *Viruses* **12**,
856 doi:10.3390/v12060642 (2020).
- 857 38 Morens, D. M. & Fauci, A. S. Emerging Pandemic Diseases: How We Got to COVID-19.
858 *Cell* **182**, 1077-1092, doi:10.1016/j.cell.2020.08.021 (2020).
- 859 39 Gordon, D. E. *et al.* A SARS-CoV-2 protein interaction map reveals targets for drug
860 repurposing. *Nature* **583**, 459-468, doi:10.1038/s41586-020-2286-9 (2020).
- 861 40 Savastano, A., Ibáñez de Opakua, A., Rankovic, M. & Zweckstetter, M. Nucleocapsid
862 protein of SARS-CoV-2 phase separates into RNA-rich polymerase-containing
863 condensates. *Nature Communications* **11**, 6041, doi:10.1038/s41467-020-19843-1
864 (2020).
- 865 41 Cascarina, S. M. & Ross, E. D. A proposed role for the SARS-CoV-2 nucleocapsid protein
866 in the formation and regulation of biomolecular condensates. *FASEB J* **34**, 9832-9842,
867 doi:10.1096/fj.202001351 (2020).
- 868 42 Ju, X. *et al.* Identification of functional cis-acting RNA elements in the hepatitis E virus
869 genome required for viral replication. *PLoS Pathog* **16**, e1008488,
870 doi:10.1371/journal.ppat.1008488 (2020).

871